Journal of Statistical Physics, Vol. 66, Nos. 1/2, 1992

Monte Carlo Study of the Effect of Perturbations on Critical Droplets

L. Monette,[1,2] W. Klein,[1] and M. Zuckermann[3]

Received February 20, 1991; final May 29, 1991

We present a Monte Carlo study of the effect of perturbations on critical or nucleation droplets in both classical and spinodal nucleation. Locating the saddle point with an intervention technique, we determine that the effect of perturbations at the saddle point depends on their location in the droplet. We find that the most effective perturbations occur at the location of the maximum growth rate where the droplet is allowed to nucleate and grow unperturbed. Moreover, the decay of sufficiently perturbed droplets follows a path that can be best characterized as a growth mode in reverse, specifically the decay of classical droplets is at the surface and that of spinodal droplets at the center independent of the location of the perturbation.

KEY WORDS: Nucleation; perturbation; growth and saddle point study.

1. INTRODUCTION

Transitions between the various phases accessible to matter are some of the most fascinating macroscopic events in nature. In particular, considerable effort has been devoted to understanding the dynamics of first-order phase transitions, i.e., metastability, nucleation, spinodal decomposition, late-stage growth, and coarsening.[1] In spite of extensive experimental and theoretical studies of first-order phase transitions, a complete theoretical understanding of this phenomenon does not as yet exist. In the case of metastability and homogeneous nucleation, a great deal of progress has been made,[2–6] and many features and predictions of theory have been verified.[7–9] However, there is little understanding of heterogeneous nuclea-

[1] Center for Polymer Studies and Physics Department, Boston University, Boston, Massachusetts 02215.
[2] Exxon Research and Engineering, Annandale, New Jersey 08801.
[3] Physics Department, McGill University, Montreal, Quebec H3A 2T8, Canada.

0022-4715/92/0100-0117$06.50/0

tion and the decay of systems very close to the limit of stability of the metastable state, i.e., the Becker–Döring limit. Heterogeneous nucleation is a technologically important process which is initiated by the presence of impurities and defects. To understand this process, it is necessary to examine the manner in which the nucleation mechanism is altered by the presence of these impurities.

In this paper we present a phenomenological approach to homogeneous nucleation which could potentially serve as a starting point for the study of some forms of heterogeneous nucleation. In our approach, defects and impurities are viewed as general perturbations and we study the effects of such perturbations on the nucleating droplet. This is in contrast to the treatment of impurities as objects that cause a reduction in the free energy barrier to nucleation. Our immediate goal is to obtain information about the effect of perturbations on the growth of critical droplets near the saddle point that separates the stable and metastable regions of phase space. Our long-range goal is to understand the effect of perturbations throughout the nucleation and growth process. This study also tests in considerable detail the accuracy of the saddle point description[2–4] of nucleation and probes the role of structures present in the system before the occurrence of the critical droplet.

The structure of the remainder of this paper is as follows. In Section 2 we briefly outline the theoretical predictions of nucleation and early-stage growth found in refs. 2–4. In Section 3 we describe our model and numerical technique. In Sections 4 and 5 we present our numerical results and finally discuss our results in Section 6.

2. THEORETICAL BACKGROUND

The approach we take was developed in refs. 2–4. We treat the metastable state essentially as an equilibrium state, which requires a certain amount of justification. The interested reader is referred to ref. 3. The aim is to calculate the partition function z,

$$z = \int \delta\phi \exp\{-\beta H(\phi)\} \tag{2.1}$$

where the integral is over all function ϕ, β is the inverse temperature, and

$$H(\phi) = \int d\mathbf{x}\{[R\nabla\phi(\mathbf{x})]^2 + \varepsilon\phi^2(\mathbf{x}) + \phi^4(\mathbf{x}) - h\phi(\mathbf{x})\} \tag{2.2}$$

In Eq. (2.2), $\varepsilon = (T - T_c)/T_c$, T_c is the critical temperature, h is an applied magnetic field, and R is the range of interaction of the potential. The

function $H(\phi)$ is the standard Landau–Ginsburg Hamiltonian.[1] In the metastable state $\varepsilon < 0$.

The critical or saddle point droplet is associated with the solution of the Euler–Lagrange equation obtained from functionally differentiating $H(\phi)$ and setting the derivative equal to zero.[3] That is,

$$R^2\nabla^2\phi(\mathbf{x}) - 2\,|\varepsilon|\,\phi(\mathbf{x}) + 4\phi^3(\mathbf{x}) - h = 0 \tag{2.3}$$

for $\phi(\mathbf{x}) = \phi_c(\mathbf{x})$ and we have made the minus sign in ε explicit.

Near the coexistence curve ($h \sim 0$) and far from the critical point the critical droplet $\phi_c(\mathbf{x})$ has the classical structure, an interior that is similar to the stable phase, and a sharp interface. Following Langer,[3] we can describe the initial growth of the droplet away from the saddle point by linearizing Eq. (2.3) around $\phi_c(\mathbf{x})$ and obtaining the eigenvector associated with the negative eigenvalue of the operator

$$R^2\nabla^2 u(\mathbf{x}) - 2\,|\varepsilon|\,u(\mathbf{x}) + 12\phi_c^2(\mathbf{x})\,u(\mathbf{x}) = \lambda u(\mathbf{x}) \tag{2.4}$$

For classical droplets the eigenvector, from Eq. (2.4), associated with the negative λ is peaked at the surface of the droplet.[3,10] This implies that the classical droplets grow by adding matter to their surface.

For systems with long-range interactions ($R \gg 1$) we expect mean field theory to be correct[11] and hence the metastable state ends at a spinodal.[4,12] The spinodal is a line of critical points[12] at which the surface tension vanishes. This leads to a significant modification in the form of the critical droplet near the spinodal.[4,5] We can modify the saddle point approach to work near the spinodal by introducing a new field

$$\psi(\mathbf{x}) = \phi(\mathbf{x}) - \phi_{\text{sp}} \tag{2.5}$$

The quantity ϕ_{sp} is the value of ϕ at the spinodal and can be obtained from the Landau–Ginsburg Hamiltonian [Eq. (2.2)] by assuming $\phi(\mathbf{x}) = \phi$ is a spatial constant and making the mean field assumption that $H(\phi)$ is a free energy. The Landau–Ginsburg free energy per spin $f(\phi)$ is

$$f(\phi) = -|\varepsilon|\,\phi^2 + \phi^4 - h\phi \tag{2.6}$$

For fixed ε, ϕ_{sp} is located by equating the second derivative of $f(\phi)$ with respect to ϕ equal to zero. The value of h at the spinodal, h_{sp}, is obtained by setting the first derivative of $f(\phi)$ with respect to ϕ equal to zero at $\phi = \phi_{\text{sp}}$.

We now insert

$$\phi(\mathbf{x}) = \psi(\mathbf{x}) + \phi_{\text{sp}} \tag{2.7}$$

into Eq. (2.2) to obtain, near the spinodal,

$$\hat{H}(\psi) = \int d\mathbf{x}\{[R\nabla\psi(\mathbf{x})]^2 + \Delta h\psi(\mathbf{x}) - \alpha\psi(\mathbf{x})\} \tag{2.8}$$

where $\Delta h = h_s - h$, α is a constant which does not vanish at the spinodal, and we have neglected the $\psi^4(\mathbf{x})$ term since $\psi(\mathbf{x}) \ll 1$ near the spinodal.[2,4]

Following the same procedure as in the classical case, we obtain the critical droplet by solving the Euler–Lagrange equation obtained from the functional differentiation of Eq. (2.8). The critical droplet near the spinodal is seen to be diffuse[4,9] with no distinction between the interior and the surface. Moreover, one can map the thermal critical phenomenon problem onto a percolation transition[4,13,14] and show that the critical or nucleating droplet is a fractal.[14,15]

Using the same technique to describe the early stage of growth as was used in the classical case, we linearize the Euler–Lagrange equation about the critical droplet to obtain an eigenvalue problem. As before, the eigenvector associated with the negative eigenvalue describes the early stage of growth. In contrast to the classical case, where the eigenvector indicates growth at the droplet surface, the eigenvector near the spinodal is peaked at the center of the droplet. This indicates that the early stage growth is a filling in of the droplet.[5,8,9]

This brief outline of the theory should be enough to understand the numerical results described in Sections 4 and 5. The reader interested in further detail is referred to refs. 2–15, particularly ref. 3 for the classical theory and ref. 5 for the spinodal.

3. NUMERICAL TECHNIQUE AND MODEL

We studied the effect of perturbations on the growth mode of a nucleating droplet using Monte Carlo methods. The simulations were performed on a two-dimensional system of Ising-like spins, with 160,000 sites. In order that the model exhibit a first-order phase transition as a function of the temperature, the spin-down state is chosen to be doubly degenerate. The Hamiltonian for such a system is given by

$$H = -\frac{J}{2}\sum_{(i,j)_q}\sigma_i\sigma_j - \frac{\Gamma - kT\ln 2}{2}\sum_i \sigma_i \tag{3.1}$$

where $\sigma_i = \pm 1$, J is the coupling constant, Γ is the energy gap between the spin states (the quantity $\Gamma - kT\ln 2$ can be interpreted as a temperature-dependent effective field), q is the number of nearest-neighbor sites, and

$(i, j)_q$ indicates the appropriate sum over these sites. The model of Eq. (3.1) exhibits a first-order phase transition at a temperature

$$kT_f = \frac{\Gamma}{\ln 2} \tag{3.2}$$

provided T_f is less than the critical temperature of the related zero-gap, nondegenerate Ising model. We used a Creutz microcanonical Monte Carlo algorithm,[16] where the total energy is conserved, and a "hopping" (not diffusive) demon redistributes the energy among the sites which are visited at random. The metastable phase is represented by a lattice configuration mostly composed up spins, whereas a configuration of mostly down spins represents the stable phase. Figure 1 displays the phase diagram for our model obtained from a mean field approximation.[9] The phase diagram is in terms of $\beta = 1/kT$ [units of $(q^J)^{-1}$] and E, where E is the energy per spin in units of qJ. It is important to note that this is not a conventional phase diagram, but a phase diagram generated on the basis of a microcanonical ensemble. It can easily be converted to a phase diagram associated with a canonical ensemble via the transformation between energy and magnetization (see ref. 9 for details). The gap energy Γ is taken to be $\Gamma = 0.27qJ$, which corresponds to a fist-order phase transition temperature of $kT_f = 0.39qJ$ [see Eq. (3.2)]. We study two cases: a system with a short-range interaction (lattice coordination number $q = 4$), for quenches (A, B, C, D, and E) reasonably close to the coexistence curve, and a system with a long-range interaction ($q = 684$), quenched reasonably close to the spinodal (quench G). The coordination number q is a measure of the inter-

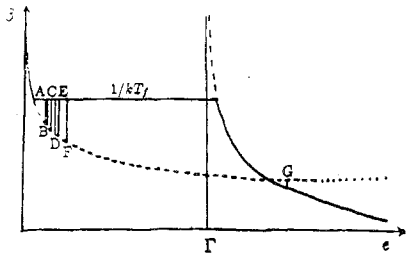

Fig. 1. Phase diagram in terms of the inverse thermal energy β vs. the energy per spin e for a gap energy $\Gamma = 0.27qJ$ and J is taken as $q/1000$. Stable branches (solid lines), metastable branches (dashed lines), and unstable branch (dotted line) as well as the coexistence curve for a transition temperature $kT_f = 0.39$ is shown. Transition A is for $q = 4$ and $e = 40$, transition B is for $q = 4$ and $e = 41$, transition C is for $q = 4$ and $e = 45$, transition D is for $q = 4$ and $e = 50$, transition E is for $q = 4$ and $e = 55$, transition F is for $q = 12$ and $e = 70$, and transition G is for $q = 684$ and $e = 370$.

action range as each spin interacts with q neighbors. The strength of the interion is scaled with q so that the energy per spin remains finite as $q \to \infty$. The details of this model for large q are presented in ref. 9.

The onset of nucleation was determined in two ways. First we monitored the center of mass[8] of the largest spin-down cluster present in the system using the correlated site-random bond clusters of Coniglio and Klein.[4,13,14] As mentioned in the previous section, this method maps Ising models including critical points and the spinodal in mean field onto a correlated site-bond percolation problem, thereby allowing us to identify correlated clusters of identical spins with thermal fluctuations. Near the spinodal, the theory predicts[4] that nucleation is initiated by the critical phenomenon fluctuations associated with the spinodal critical point. We identify the occurrence of a nucleating cluster as the point at which the location of the center of mass of the largest of the clusters associated with spinodal fluctuations ceases to exhibit large fluctuations, i.e., when the fluctuations in the position of the droplet center of mass are within the droplet correlation length. For the classical case we use the same method with the same cluster definition. Away from critical points these percolation clusters are compact and the identification of the classical critical droplets with these clusters gives good agreement in measurement of nucleation rates near the coexistence curve.[17] We refer to this precedure as the center-of-mass method and it is described in detail in ref. 9.

If, however, we define the onset of nucleation with the appearence of a saddle point structure,[2-4] then the center-of-mass method is not sufficient. The saddle point structure is roughly a droplet that just makes it to the top of the saddle point separating the stable and metastable states in phase space.[3] We can identify this droplet by using the fact that a saddle point structure should initiate the decay of the metastable state in only 50% of trials. In the other half of the trials the saddle point structure itself should decay and the system remain in the metastable state.

We identify the saddle point structure or droplet by using the intervention method in conjunction with the center-of-mass method. The intervention technique involves stopping the simulation when a large and stable spin-down cluster is present in the system, changing the random number seed, and restarting the simulation. The largest cluster is subsequently monitored until it decays or grows. This process is repeated several times with the same initial simulation. The saddle point droplet is taken to be the cluster which, in a reasonable number of such trials, decayed in roughly half of these trials. If the trial cluster decays in more than 50% of the tests, the original simulation is allowed to proceed further before the intervention takes place. If the trial cluster decays less than 50% of the time, the intervention is tried earlier in the simulation. These two criteria for nucleation,

the center-of-mass method and the intervention method, give the same result for the time of nucleation near the spinodal, but quite different results in the classical case. We discuss these results in the next section.

4. NUMERICAL RESULTS; TIME LAG

The center-of-mass and the intervention method give similar results for the occurrence of a critical droplet for systems with long-range interactions ($q = 684$) near the spinodal. However, far from the spinodal for both long- and short-range interactions ($q = 4$) the center-of-mass method leads to the conclusion that there is a stable monotonically growing structure in the system long before the saddle point is reached. That is, "center-of-mass nucleation" occurs much earlier than nucleation as determined by the intervention method.

We studied the "time lag" between nucleation as determined by the two methods for various quench depths ($q = 4$ for quenches A, B, C, D, and E; $q = 12$ for quench F; and $q = 684$ for quench G) and the results are summarized in Table I. We observe that the time lag between nucleation events as determined by the two methods decreases as the quench depth increases. We postulate that this effect is due to the compact structure of classical nucleating droplets as opposed to the fractal nature of the droplets near the spinodal.[4,9,15] The center-of-mass method far from the spinodal, where classical nucleation is expected,[4,9,18] appears to measure the occurrence of an apparently stable compact cluster well before that cluster becomes the saddle point (nucleating) droplet. In other, words a monotonically growing cluster dominates the system in the sense that it will remain the largest cluster for the remainder of the run, long before that cluster reaches the saddle point.

Table I.

Energy	Coordination number q	Lag time	Average size $\langle s \rangle$	Number of trials
40	4	480	230	1[a]
41	4	230 ± 30	180 ± 11	3[a]
45	4	125 ± 30	114 ± 10	5
50	4	98 ± 19	103 ± 10	5
55	4	32 ± 12	79 ± 14	5
70	12	~ 10	—	5
370	684	~ 0	—	5

[a] Fewer than five trials due to the long waiting times for the onset of nucleation.

We did not observe this effect near the spinodal. We believe that this is due to the increasingly diffuse nature of the droplets present in the system. The center-of-mass method does not indicate the occurrence of a stable structure in the system prior to a saddle point droplet because a fractal object is more easily destroyed by thermal fluctuations than a compact object. Close to the spinodal, the first appearance of a stable monotonically growing cluster will coincide with the system reaching the saddle point or the diffuse droplet will be destroyed by fluctuations. We believe that the diffuse nature of the critical droplet is the reason that both methods, center of mass and saddle point, agree with each other as the quench depth increases.

If the time lag can be explained in terms of the structure of the nucleating droplet, we then propose that this effect can be treated as a signature of classical nucleation and can be used as an additional criterion in computer simulations where the exact nature of the nucleation phenomenon taking place (i.e., whether it is classical or nonclassical) has not been determined. In order to verify that the existence of this "time lag" is not an artifact of the Creutz algorithm, we measured the "time lag" for quench C (see Fig. 1) using a Glauber algorithm. The results were found to be the same as those displayed in Table I.

5. NUMERICAL RESULTS; PERTURBATIONS

We turn now to the question of the effect of perturbations on the saddle point droplet. In this section the term droplet will always refer to the saddle point nucleation event.

Several perturbations were used to test the stability of nucleating droplets for both $q = 4$ (quench C) and $q = 684$ (quench G) in Fig. 1. They all consist of removing down spins in a circular shell located at a distance r from the center of mass of the droplet. The number of spins removed from the system remains constant for each shell and consequently the thickness of the shell depends on its distance from the center of mass of the droplet (see Fig. 2). Figure 3 shows the measured density profile of the nucleating droplets as determined by the intervention method for (a) $q = 4$ and (b) $q = 684$ near the spinodal, respectively. The bars of the histogram superimposed on the density profile represent the fraction of the trials in which the droplet decayed due to a perturbation. This fraction was rescaled by factor of $\frac{1}{2}$ (with a *random* perturbation, the nucleating droplet should decay in a fraction $f = \frac{1}{2}$ of the trials) and renormalized to an arbitrary height. The location of a particular bar of the histogram indicates the location of the corresponding perturbation shell. Since the perturbation shells become very narrow at large distances from the center of the droplet, many

shells in a given interval were averaged into a single bar of the histogram. Finally, each bar of the histograms represents 10 trials for $q=4$ and 16 trials for $q=684$.

We compare Figs. 3a and 3b to the numerical solution of the predicted eigenvector from the theory,[10] which is reproduced in Fig. 4. The qualitative agreement between the features of the numerical solution and our results is excellent, except for the noise in the density profile of Fig. 3b for regions close to the center of the droplet. This noise is due to the relatively small area of the annuli over which the density average was taken near the droplet center. As an example of the agreement between the eigenvector interpretation and the numerical results, in Fig. 4 the eigenvector in classical nucleation extends well beyond the classical droplet profile, but its amplitude becomes extremely weak. A corresponding feature of all our simulation results is that the classical nucleating droplet is not very sensitive to perturbation of its exterior. Moreover, the histogram data in

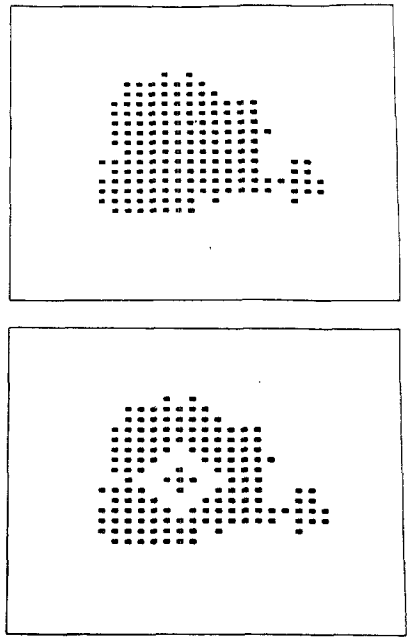

Fig. 2. Example of a peturbation [2–3]. The top figure represents the unperturbed nucleating droplet. The bottom figure represents the same nucleating droplet after the perturbation [2–3] where all the 20 spins in the "diamond-shaped" ring between the distances $r=r_i+r_j=2$ and $r=r_i+r_j=3$ inclusively have been removed. The subscripts i and j refer to the x and y directions.

Figs. 3a and 3b reproduce the shape of the eigenvector for classical and nonclassical nucleation, respectively.

Consideration of these results leads us to propose the following interpretation of the role of the eigenvector in the decay processes of the nucleating droplet. The extent to which a perturbation destroys a nucleat-

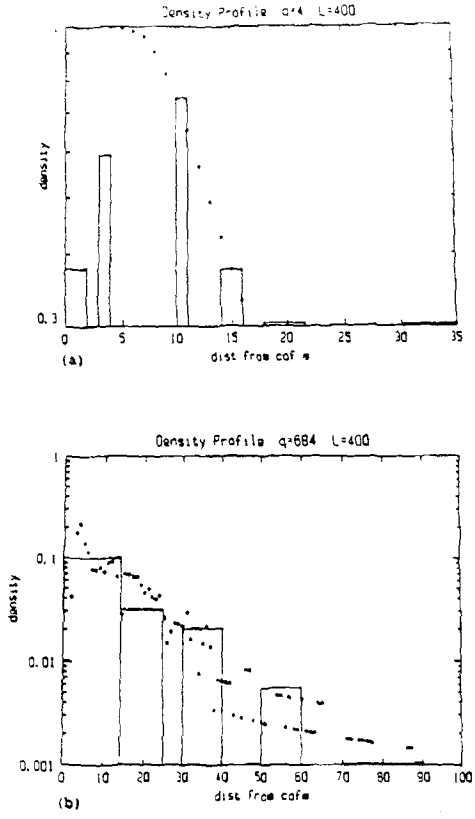

Fig. 3. Semilog plots of the measured density profile of the nucleating droplets as determined by the intervention method in terms of the logarithm of the density versus the distance. (a) For quench C, (b) for quench G. The bars of the histograms superimposed on the density profile plot, which have been rescaled to an arbitrary height, represent the fraction f of the trials in which the droplet decayed due to a perturbation. The largest histogram bar in each figure corresponds to case when all the perturbed droplets decayed. A given perturbation involved removing a total of 13 spins in (a) and a total of 52 spins in (b). The fraction f was rescaled to an arbitrary height independent of the y axis of these plots. The x coordinate of a particular bar of the histogram represents the location of the "ring" from which the down spins are removed. Bars of the histogram far away from the center of the droplet represent an average over many neighboring "rings." Each bar of the histogram represents an average over 16 trials in both (a) and (b) and the relative heights represent the relative efficiency, *above a random perturbation*, of the controlled perturbation.

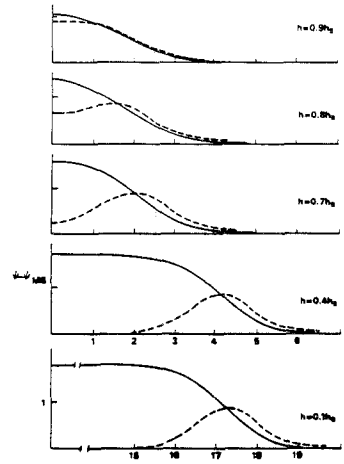

Fig. 4. Plot of the profiles of the nucleating droplet (solid line) and the growth mode (dashed line) in three dimensions.

ing droplet is related to its projection onto the predicted eigenvector. For instance, a perturbation located at the interface of a classical nucleating droplet is most effective, while the same perturbation (same number of spins removed) located at the center is statistically much less effective than at the interface and a perturbation located outside the droplet is statisti-

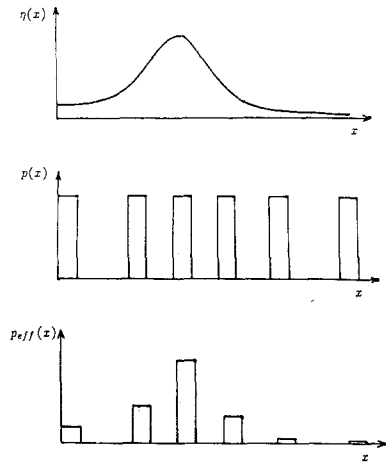

Fig. 5. (a) The eigenvector for a classical saddle point droplet. (b) Schematic illustration of the applied perturbations as a function of distance away from the center of the droplet. (c) Illustration of the effective perturbation $p_{\text{eff}}(x)$, i.e., $p(x)$ in b) projected onto the eigenvector $\eta(x)$ in (a).

cally even less effective. Similarly, a perturbation of the center of a non-classical (spinodal) droplet is most effective, while a perturbation far away from the center has very little effect.

Figure 5 schematically illustrates the above statement. Figure 5a shows the shape of the eigenvector as a function of the distance from the center of mass of the droplet for classical nucleation and Fig. 5b gives the original perturbation as a function of the distance from the center of mass of the droplet. The equal height of the bars implies that the number of spins removed remains constant as a function of distance. Figure 5c shows the actual sensitivity of the droplet to the applied perturbation shown in Fig. 5b, as "controlled" by the shape of the corresponding eigenvector of Fig. 5a.

Put in a concise form, we propose that the effect of a perturbation p_{eff} is roughly proportional to

$$p_{\text{eff}}(r) \propto \int dr\, p(r)\, \eta(r) \tag{5.1}$$

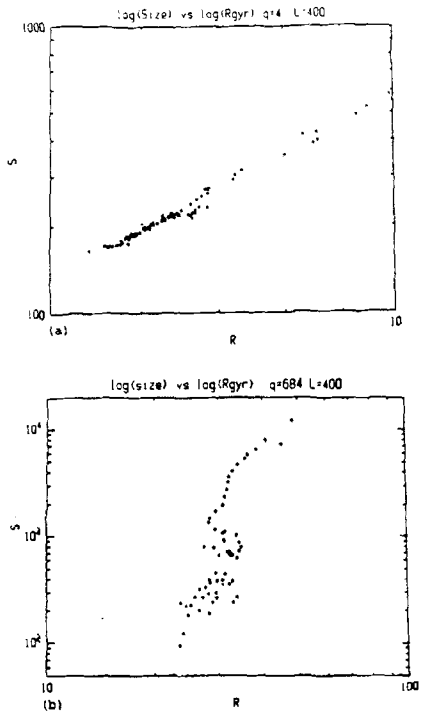

Fig. 6. Initial growth mode of the nucleating droplet in terms of a plot of the logarithm of the total mass of the droplet S as a function of the logarithm of its radius of gyration R_{gyr}. (a) For quench C, b) for quench G.

where $p(r)$ symbolizes a spherically symmetric perturbation, r is measured from the center of the nucleating droplet, and $\eta(r)$ represents the eigenvector. The above relation is only qualitative. However, it may be useful as a starting point in the study of some forms of heterogeneous nucleation.

The eigenvector not only indicates where a perturbation of a given size is most efficient, but it also appears to indicate the mode of decay of the perturbed droplet. In Langer's description[3] of early-stage growth in classical nucleation, the peak of the eigenvector is at the surface of the droplet (see Fig. 4). In Fig. 6a the log of the mass of the critical droplet is plotted as a function of the radius of gyration of the droplet. Each point from the lower left to the upper right of the figure is taken at a later time. If the droplet is growing classically, this plot should be a straight line with slope d, the spatial dimension. The slope of the line in Fig. 6a is 2, which is the spatial dimension used in the simulation. In spinodal nucleation the eigen-

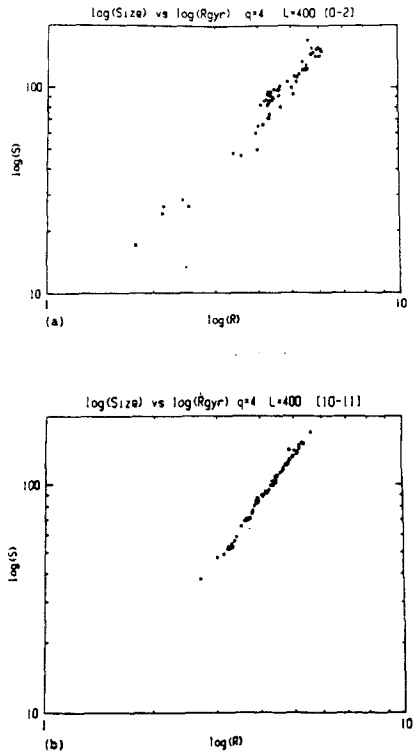

Fig. 7. Plots of the logarithm of the size of droplet C ($q=4$, $e=45$) vs. the logarithm of its radius of gyration. (a) For a perturbation around the center ([0–2]), (b) for a perturbation around the interface ([10–11]). Both plots display a slope of 2, and they have been averaged over 5 trials.

vector is peaked in the center (Fig. 4), which indicates that the growth should be a filling-in process. In Fig. 6b we plot the log of the droplet mass vs. the log of the radius of gyration for a droplet near the spinodal. The initial growth is a large increase in mass with almost no change in the radius of gyration. As above, each point from lower left to upper right represents a later time. This figure is in qualitative agreement with the theory.

In Fig. 7 we plot the decay of a classical droplet. In this figure time runs from the upper right-hand corner to the lower left. Again we show the mass of the droplet as a function of the radius of gyration. As with the growth in Fig. 6a, we have a straight line with slope 2, indicating that the decay is occurring at the surface *independent of the location of the perturbation.* Figure 7a corresponds to a perturbation at the center, while Fig. 7b results from a perturbation at the interface.

In Fig. 8 we have a similar plot for spinodal nucleation. As with growth near the spinodal, the decay occurs at the center of the droplet

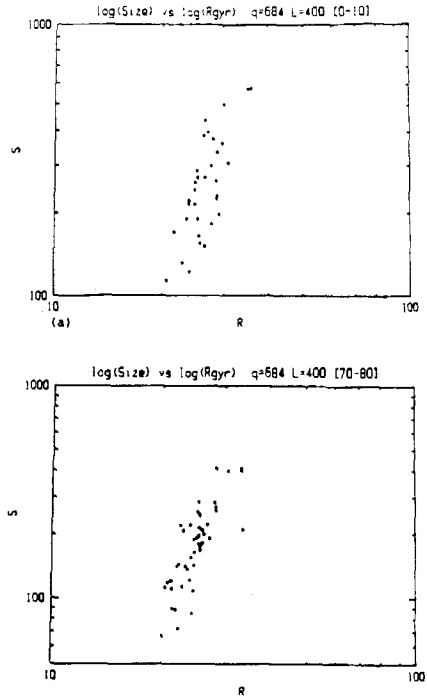

Fig. 8. Plots of the logarithm of the size of droplet G ($q = 684$, $e = 370$) vs. the logarithm of its radius of gyration. (a) For a perturbation around the center ([0–10]), b) for a perturbation around the end part of the interface ([70–80]). Both plots have been averaged over 5 trials.

independent of the location of the perturbation. Figure 8a results from a perturbation at the droplet center, while Fig. 8b shows the effect of a perturbation near the outer edge.

Similar results to those presented in Figs. 7 and 8 were also obtained from runs using a Metropolis and a Kawasaki algorithm.[18] These results imply that the location of the decay mode and its invariance with respect to the location of the perturbation are not affected by the conservation laws.

6. CONCLUSIONS AND DISCUSSION

Our results can be summarized as follows: In nucleation close to the coexistence curve in systems with either long- or short-range interactions, monotonically growing clusters can be identified long before they obtain the status of saddle point droplets. This does not appear to be true for nucleation near the spinodal, where the saddle point droplet is the first stable growing structure that can be identified. We attribute this difference to the compact structure of the droplets near the coexistence curve and the diffuse fractal structure of the droplets near the spinodal. Moreover, the time lag between the stabilization of the location of the center of mass and the saddle point decreases as the distance of the quench from the coexistence curve increases.

We also examined the affect of perturbing droplets near the saddle point. We found that classical droplets decayed at the surface and spinodal droplets decayed at the center independent of the location of the perturbation within the droplet. However, the efficiency of the perturbation in destroying droplets did depend on its location within the droplet. Perturbations of the same number of spins were more efficient if located near the interface of a classical droplet rather than the center, while the reverse was true of spinodal droplets.

We have not performed simulations to test the effect of adding rather than deleting spins from the critical droplet in the direction of the stable phase. However, the symmetry of the saddle point evident in the theoretical work of Langer[3] and the simulations performed in this work make it highly likely that such additions will result in an enhancement of nucleation qualitatively similar to the reduction of nucleation seen here.

The purpose of this work was to begin to investigate how the nucleation process can be manipulated and how it might be affected by external influences. Clearly we are still a long way from an understanding of the effect of "dirt" in heterogeneous nucleation. We believe, however, that a thorough understanding of the role of droplet structure in the response to perturbations will be important for an understanding of this phenomenon.

ACKNOWLEDGMENTS

This work was supported by grants from the ONR, NSF, NSERC and the FCAR du Québec.

REFERENCES

1. J. D. Gunton, M. San Miguel, and P. S. Sahni, in *Phase Transitions and Critical Phenomena*, Vol. 8, C. Domb and J. L. Lebowitz, eds. (Academic, New York, 1983).
2. J. W. Cahn and J. E. Hilliard, *J. Chem. Phys.* **28**:256 (1958).
3. J. S. Langer, *Ann. Phys.* **41**:108 (1967).
4. W. Klein and C. Unger, *Phys. Rev. B* **28**:445 (1983).
5. C. Unger and W. Klein, *Phys. Rev. B* **29**:2698 (1984).
6. K. Binder, *Phys. Rev. A* **29**:341 (1984).
7. D. Stauffer, A. Coniglio, and D. W. Heermann, *Phys. Rev. Lett.* **49**:1299 (1982).
8. D. W. Heermann and W. Klein, *Phys. Rev. Lett.* **50**:1062 (1983).
9. L. Monette, W. Klein, M. J. Zuckermann, A. Khadir, and R. Harris, *Phys. Rev. B* **38**:11607 (1988).
10. C. Unger and W. Klein, *Phys. Rev. B* **31**:6127 (1985).
11. J. L. Lebowitz and O. Penrose, *J. Math. Phys.* **7**:98 (1966).
12. D. W. Heermann, W. Klein, and D. Stauffer, *Phys. Rev. Lett.* **49**:1261 (1982).
13. A. Coniglio and W. Klein, *J. Phys. A* **13**:2775 (1980).
14. W. Klein, in *Computer Simulations in Condensed Matter Physics 3*, D. P. Landau, K. K. Mon, and H. B. Schütter, eds. (Springer-Verlag, Heidelberg, 1991).
15. T. S. Ray and W. Klein, *J. Stat. Phys.* **31**:891 (1990).
16. M. Creutz, *Phys. Rev. Lett.* **50**:1411 (1983).
17. D. W. Heermann, A. Coniglio, W. Klein, and D. Stauffer, *J. Stat. Phys.* **36**:447 (1984).
18. L. Monette, Ph.D. thesis, Boston University, Boston, Massachusetts (1990).